Research Square

Preprints are preliminary reports that have not undergone peer review.
They should not be considered conclusive, used to inform clinical practice,
or referenced by the media as validated information.

Petrology and geochemistry of I-type granitoids from the Makassa area, Far North Cameroon: new insights into late-orogenic Pan-African magmatism along the Mayo-Kébbi arc

Amadou Diguim Kepnamou

kepnamoudiguim@yahoo.fr

University of Garoua

Ganwa Alembert Alexandre

University of Ngaoundéré

Naïmou Seguem

University of Moundou

Ngounouno Ismaïla

University of Ngaoundéré

Research Article

Keywords: Pan-African Fold Belt, I-type granitoids, Post-collisional magmatism, North Cameroon domain, Central African Fold Belt, Makassa

Posted Date: November 3rd, 2026

DOI: https://doi.org/10.21203/rs.3.rs-11292956/v1

License: This work is licensed under a Creative Commons Attribution 4.0 International License.
Read Full License

Additional Declarations: No competing interests reported.

Abstract

The Makassa area, in the North Cameroon domain of the Central African Fold Belt (CAFB), preserves Pan-African plutonic and metamorphic rock whose petrogenesis and geodynamic significance remain poorly constrained. We present petrographic and whole-rock geochemical data for 12 representative samples (selected from 22 collected) of amphibole-biotite granite, biotite granite, gneiss and amphibolite. The rocks form a continuous compositional series (53.83–74.97 wt% SiO_2); the gneiss and amphibolite are ortho-derived and are treated together with the plutonic suite. Decreasing Al_2O_3, Fe_2O_3, MgO, CaO and TiO_2 with increasing SiO_2 is consistent with fractional crystallization of amphibole, biotite, plagioclase, Fe-Ti oxides and apatite from a common parental magma. The granitoids are predominantly metaluminous, ferroan, high-K calc-alkaline to shoshonitic I-type rocks (A/CNK = 0.79–1.17), with one peraluminous S-type sample. They show LREE enrichment, flat HREE segments, negative Eu anomalies (Eu/Eu* = 0.10–0.47) and depletion in Ba, Nb-Ta, Sr and Ti, indicating a dominantly crustal, tonalitic-granodioritic source with a subordinate mantle contribution. In Rb versus (Y + Nb) and Rb versus (Ta + Yb) diagrams the samples plot across the volcanic-arc, syn-collisional and within-plate fields, a pattern interpreted as a post-collisional setting that inherits an arc-like source signature. The Makassa magmatism therefore records the transition from a late-collisional to a post-collisional stage of the Pan-African orogeny. These data provide the first geochemical characterization of Pan-African magmatism in the Far North Cameroon sector of the Mayo-Kébbi/North Cameroon arc, previously known only from Rb/Sr ages.

1 Introduction

The Central African Fold Belt (CAFB), also referred to as the Central African “mobile zone” [1–3] or the North Equatorial Pan-African Belt [4], is an E-W-trending orogenic belt more than 5000 km long and about 300 km wide. It extends from Nigeria through Cameroon and Chad to the Central African Republic [5–7], and separates the Congo Craton to the south, the West African Craton to the west and the Saharan Metacraton to the north [8–13] (Fig. 1). Before the opening of the South Atlantic, the CAFB continued into the Borborema Province of northeastern Brazil [14–18].

In Cameroon, the CAFB is divided into three structural domains [19]: the Southern, Central and Northern domains, the last comprising the Northwest Cameroon and Mayo-Kébbi sub-domains [20]. Its geodynamic evolution reflects the relative motion of several cratonic blocks, namely the Congo-São Francisco Craton, the West African Craton and a Neoproterozoic domain comprising the Hoggar, Nigeria, the Borborema Province and the polycyclic basement of Central Africa [8, 15], together with interactions between the Congo-São Francisco Craton and the Saharan Metacraton [21–23]. An alternative model invokes microplate convergence marked by two submeridian suture zones: the southern Aïr-Tirririne suture, marked by an ophiolitic complex [24, 25], and the Massénya-Ounianga suture in Chad, evidenced by a positive gravity anomaly [26, 27]. The Tcholliré-Banyo shear zone, about 150 km long, is generally interpreted as the Cameroonian continuation of this gravity anomaly. It corresponds to the Rey Bouba

greenstone belt, which is associated with a Neoproterozoic subduction zone separating the North Cameroon Domain from the Adamawa-Yadé Domain.

The Mayo-Kébbi Domain is a NE-SW trending magmatic arc that extends from the Gouna-Sinassi area (North Cameroon) to the Makassa area (Far North Cameroon), passing through the Mayo-Kébbi region of southwestern Chad. The northern Cameroonian and southwestern Chadian sectors of this arc have been the subject of numerous petrographic, structural, geochemical, geochronological and isotopic studies. For Far North Cameroon, however, the only available geochronological data are the whole-rock Rb/Sr ages of 626 ± 15 Ma and 677 ± 40 Ma obtained by Lasserre [28] on the deformed Kaélé granites. Knowledge of this sector therefore relies largely on extrapolation from studies of the more southerly domains [20, 29–32].

This study addresses this gap by presenting new petrographic and whole-rock geochemical data from the Makassa area. Its objectives are to characterize the source and origin of the magmatism, to clarify the associated geodynamic setting, and to discuss the evolution of this part of the Mayo-Kébbi Domain crust during the Pan-African orogeny.

2 Geological setting

Cameroon lies in Central Africa at the head of the Gulf of Guinea. It is bounded by Chad to the north, the Central African Republic to the east, Congo, Gabon and Equatorial Guinea to the south, and Nigeria to the west. About one third of the country consists of Pan-African formations belonging to the Central African Pan-African Mobile Zone [2], which is divided into three tectonic domains: the Yaoundé Domain, the Central (Adamawa-Yadé) Domain and the North Cameroon Domain [19]. This study concerns only the North Cameroon Domain.

The North Cameroon Domain lies west of the Tcholliré-Banyo Fault. It extends into Nigeria, includes the Poli region of Cameroon and the areas north of Garoua [19, 33], and continues into the Mayo-Kébbi region of Chad [20, 34]. This segment of the Pan-African chain has been studied extensively [6, 29, 35]. Its basement is overlain by Upper Proterozoic metasedimentary and metavolcanic rocks (U/Pb zircon age of about 830 Ma). The domain also contains calc-alkaline granitoids dated at about 530 Ma and post-tectonic alkaline granites [36], whose emplacement marks a major magmatic event of the Pan-African orogeny.

Three deformation phases (D1-D3) have been recognized [6, 36]. D1 is characterized by tangential tectonics that produced early planar (S1) and linear (L1) structures and folds (P1), and reflects the initial stage of continental collision. D2 corresponds to sinistral strike-slip movements oriented N-S or WSW-ENE; these transcurrent faults accommodated lateral displacement during a transitional stage of the belt's evolution. D3 is marked by E-W shear zones, generally associated with drag folds with E-W or N-S axes, and records the final stages of orogenic adjustment and crustal stabilization.

The Makassa area lies within this structural framework (Fig. 2) and exposes a heterogeneous plutonic and metamorphic assemblage. The plutonic suite comprises amphibole-biotite granite and biotite granite, and the metamorphic assemblage comprises gneiss and amphibolite. These lithologies record the polyphase tectonic and metamorphic history of the Pan-African orogeny in the region.

3 Materials and methods

3.1 Sampling and petrography

Twenty-two rock samples were collected from the various lithological units of the Makassa area. Twelve fresh, unweathered samples were selected for petrographic and geochemical analysis so as to cover the full range of rock compositions observed in the field. Thin sections were prepared at the Geological and Mining Research Institute (IRGM), Yaoundé, and examined under a polarizing microscope at the Mines and Geology Laboratory of the School of Geology and Mining Engineering, University of Ngaoundéré. Modal proportions were estimated semi-quantitatively using visual comparison charts and repeated point counts across the thin sections (typical uncertainty ± 5 vol%). Alteration features were described qualitatively, and crystallization sequences were inferred from the textural and cross-cutting relationships among primary and secondary phases.

3.2 Whole-rock geochemistry

Samples representative of each lithological type were crushed, pulverized and analysed for major, trace and rare earth elements at ACME Analytical Laboratories (Vancouver, Canada). For each sample, 200 mg of powder was mixed with 900 mg of lithium metaborate ($LiBO_2$) flux, fused and dissolved in nitric acid (HNO_3). Major elements were determined by inductively coupled plasma atomic emission spectrometry (ICP-AES) and are reported as weight per cent oxides. Trace and rare earth elements were determined by inductively coupled plasma mass spectrometry (ICP-MS) and are reported in parts per million (ppm). Quality control included certified reference materials, duplicates and blanks. Analytical precision was better than ± 2% for major elements, ± 5% for trace elements above 10 ppm and ± 10% for trace elements below 10 ppm.

4 Results

4.1 Petrography

Field and petrographic investigations show that the Makassa area comprises four main rock types: amphibole-biotite granite, biotite granite, gneiss and amphibolite (Fig. 3). Their outcrop and microscopic features are illustrated in Fig. 4.

4.1.1. Plutonic rocks

- **Amphibole-biotite granite**

This rock crops out as slabs and blocks in the Makassa savanna (Fig. 4a) and has a grey to pinkish weathering patina. Biotite, quartz and orthoclase are visible to the naked eye in a granular matrix. Under the microscope the rock has a granular texture (Fig. 4b) and consists of amphibole, biotite, quartz, plagioclase, orthoclase and opaque minerals. Amphibole (15%) is green hornblende forming subhedral to anhedral crystals 0.5–1.5 mm in size, locally altered to epidote. Biotite (15%) occurs as elongated light- to dark-brown flakes 0.2–1.5 mm long and is associated with amphibole. Quartz (20%) is subhedral to anhedral (0.2-1 mm), shows undulatory extinction and is always associated with feldspar. Orthoclase (25%) forms subhedral to anhedral crystals 0.5-5 mm across, some with simple Carlsbad twins (Fig. 4c). Plagioclase (10%) occurs as patches of subhedral crystals 1-1.5 mm in size. Epidote (4%) and chlorite (2%) are secondary minerals. Opaque minerals (4%) are small dark crystals that occur as inclusions in orthoclase and other minerals.

- **Biotite granite**

This rock crops out as decimetric to metric slabs and blocks in the savanna of the Makassa area (Fig. 4d) and has a grey, yellowish to locally pinkish weathering patina. In thin section it has a granular texture (Fig. 4e) and is composed of biotite, quartz, plagioclase, orthoclase, microcline, chlorite, apatite and opaque minerals. Biotite (about 18%) forms dark-brown flakes 0.2-1 mm long, associated with feldspars and opaque minerals, and is locally altered to chlorite (3%). Quartz (25%) forms subhedral to anhedral crystals (0.1-2 mm) and polycrystalline patches with undulatory extinction, associated with the feldspars. Plagioclase (15%) forms subhedral crystals 0.5–1.5 mm long that are altered to sericite. Orthoclase (15%), the dominant alkali feldspar, forms subhedral crystals of similar size to plagioclase and is associated with plagioclase and opaque minerals. Microcline (10%), recognized by its tartan twinning (Fig. 4f), is 0.5-5 mm in size and contains inclusions of biotite, quartz and opaque minerals. Apatite is an accessory phase, and opaque minerals (10%) occur as inclusions in plagioclase and microcline.

4.1.2. Metamorphic rocks

- **Gneiss**

The gneiss crops out as slabs and blocks along the banks and bed of the watercourse. It has a schistose structure (Fig. 4g) and a thin, grey to whitish weathering patina. Microscopically it has a lepidoblastic texture (Fig. 4h) and consists of amphibole, biotite, plagioclase, orthoclase, quartz and opaque minerals. Amphibole (15%) is green hornblende, subhedral to anhedral, about 1.5 mm in size. Biotite (10%) forms elongated light- to dark-brown flakes 0.4–1.5 mm long, associated with amphibole (Fig. 4h) and locally altered to chlorite. Quartz (20%) forms subhedral to anhedral crystals 0.2-1 mm in size with undulatory extinction, generally associated with orthoclase, plagioclase and opaque minerals. Plagioclase (20%) forms patches of subhedral to anhedral crystals 0.8–2.5 mm in size, with polysynthetic twins that terminate in a wedge shape. Orthoclase (25%) forms subhedral to anhedral crystals 0.2-2 mm in size, associated with quartz and often containing opaque inclusions. Opaque minerals (about 10%; Fig. 4i) are the dark phases of the rock.

- **Amphibolite**

The amphibolite crops out in the streambed as centimetric slabs and blocks (Fig. 4j). In hand specimen it is dark with a grey weathering patina. Under the microscope it has a granoblastic texture (Fig. 4k) and consists of amphibole, quartz, orthoclase, plagioclase and opaque minerals. Amphibole (60%) is green hornblende, subhedral to anhedral (0.5-2 mm), with submicroscopic and feldspar inclusions. Quartz (15%) is subhedral to anhedral (0.5–2.5 mm), shows undulatory extinction and is associated with orthoclase and plagioclase. Plagioclase (10%) forms patches of crystals 1-1.5 mm in size with polysynthetic and albite twins (Fig. 4l). Orthoclase (10%) is perthitic and subhedral, of almost the same size as plagioclase. Opaque minerals (5%) occur as inclusions in amphibole and feldspars.

4.2 Geochemistry

The whole-rock major- and trace-element compositions of the 12 samples are given in Tables 1 and 2.

Table 1
Whole-rock major (wt%) and trace-element (ppm) compositions of the amphibole-biotite granites and biotite granites of the Makassa area

Petrology	**Amphibole-biotite granite**				**Biotite granite**			
Sample	**Mak3**	**Mak4**	**Mak6**	**Mak7**	**Mak1**	**Mak2**	**Mak5**	**Mak9**
Major elements (wt%)								
SiO_2	73.84	74.90	72.34	74.97	71.90	70.80	70.65	70.46
TiO_2	0.18	0.08	0.23	0.04	0.26	0.32	0.22	0.47
Al_2O_3	13.48	13.52	14.15	14.74	12.94	13.64	14.08	14.09
Fe_2O_3	1.89	1.54	1.14	1.36	3.87	3.56	3.64	4.26
MgO	0.56	0.05	1.01	0.09	0.48	0.42	0.62	0.68
CaO	0.82	0.95	2.05	1.39	3.78	4.28	4.21	2.21
Na_2O	3.73	3.70	3.64	4.05	2.84	2.82	2.56	4.25
K_2O	5.24	5.13	4.84	3.17	3.52	3.86	3.82	3.01
MnO	0.05	0.05	0.25	0.02	0.14	0.14	0.12	0.07
P_2O_5	0.04	0.01	0.01	0.03	0.07	0.05	0.06	0.16
Sum	99.83	99.93	99.66	99.86	99.80	99.89	99.98	99.66
LOI	0.15	0.07	0.35	1.12	0.70	0.90	0.04	0.07
Ratios and indices								
A/NK[a]	1.14	1.16	1.26	1.46	1.52	1.55	1.68	1.37
A/CNK[a]	1.01	1.01	0.94	1.17	0.84	0.82	0.88	0.99
Na_2O+K_2O	8.97	8.83	8.48	7.22	6.36	6.68	6.38	7.26
Na_2O/K_2O	0.71	0.72	0.75	1.28	0.81	0.73	0.67	1.41
FeOt[b]	1.87	1.52	1.12	0.36	3.83	3.52	3.66	4.11

[a] A/NK = $Al_2O_3/(Na_2O + K_2O)$ and A/CNK = $Al_2O_3/(CaO + Na_2O + K_2O)$, in moles

[b] FeOt = total iron expressed as FeO

[c] N = normalized to the values of McDonough and Sun [45]

Petrology	Amphibole-biotite granite				Biotite granite			
Sample	**Mak3**	**Mak4**	**Mak6**	**Mak7**	**Mak1**	**Mak2**	**Mak5**	**Mak9**
Major elements (wt%)								
Rb/10	22.13	24.37	23.68	20.29	10.85	11.25	12.89	6.85
Ta×3	6.60	9.00	8.70	7.20	2.40	3.60	2.40	2.70
MgO/CaO	0.20	0.09	0.49	0.06	0.14	0.10	0.12	0.31
P_2O_5/TiO_2	0.22	0.13	0.04	0.75	0.27	0.16	0.27	0.34
Trace and rare earth elements (ppm)								
Cs	1.70	3.20	1.20	1.60	4.20	3.80	3.60	0.80
Rb	221.30	243.70	236.80	202.90	108.50	112.50	128.90	68.50
Ba	331.00	24.00	999.00	485.00	821.00	775.00	910.00	560.00
Sr	67.20	10.30	78.70	74.30	108.90	88.30	120.70	160.90
Pb	10.10	6.00	8.10	10.00	10.90	10.10	10.30	1.70
Th	25.80	21.40	20.20	25.80	15.60	18.20	25.60	8.50
U	5.30	6.50	5.40	6.30	2.60	4.60	2.40	1.80
Zr	195.80	109.20	121.40	110.20	212.80	208.60	200.20	381.70
Hf	6.50	4.90	4.50	4.90	5.60	6.50	4.50	11.50
Ta	2.20	3.00	2.90	2.40	0.80	1.20	0.80	0.90
Y	30.10	49.40	41.60	49.20	25.70	20.30	22.80	43.00
Nb	24.70	39.60	28.40	36.90	11.00	13.70	20.20	24.90
Sc	2.00	2.00	4.00	3.00	4.00	3.00	3.00	5.00
Cr	19.00	20.00	17.00	19.00	19.00	20.00	19.00	20.00
Ni	20.00	22.00	19.00	20.00	21.00	20.00	17.00	20.00
Co	0.70	0.20	0.60	0.40	3.60	2.80	1.60	5.60
V	9.00	11.00	16.00	12.00	14.00	12.00	10.00	32.00

[a] A/NK = $Al_2O_3/(Na_2O + K_2O)$ and A/CNK = $Al_2O_3/(CaO + Na_2O + K_2O)$, in moles

[b] FeOt = total iron expressed as FeO

[c] N = normalized to the values of McDonough and Sun [45]

Petrology	Amphibole-biotite granite				Biotite granite			
Sample	**Mak3**	**Mak4**	**Mak6**	**Mak7**	**Mak1**	**Mak2**	**Mak5**	**Mak9**
Major elements (wt%)								
W	0.70	1.70	1.30	1.70	0.70	0.70	0.90	0.80
Ga	20.20	21.30	22.10	20.80	13.30	11.90	16.10	21.10
Zn	43.00	298.00	88.00	104.00	68.00	56.00	42.00	48.00
Cu	1.80	9.80	6.90	6.70	5.30	6.50	5.70	6.70
La	62.40	24.70	26.40	32.20	27.00	29.40	27.20	24.20
Ce	118.10	55.50	112.80	98.40	53.40	54.80	55.20	52.60
Pr	12.37	6.91	7.00	9.90	5.90	6.00	6.90	5.50
Nd	40.90	26.20	22.20	24.90	21.40	20.60	22.80	20.80
Sm	7.12	6.94	7.02	6.84	4.21	6.14	5.31	5.63
Eu	0.85	0.24	0.26	0.24	0.81	0.83	0.85	0.82
Gd	5.59	7.50	5.42	5.64	4.13	5.32	5.68	4.98
Tb	0.91	1.33	0.99	1.02	0.68	0.72	0.78	0.76
Dy	5.14	8.33	8.04	6.89	4.04	5.02	5.12	5.08
Ho	1.02	1.81	1.08	1.56	0.88	1.06	0.98	1.64
Er	3.09	5.50	5.20	5.56	2.84	4.22	4.14	4.06
Tm	0.46	0.79	0.68	0.76	0.42	0.48	0.42	0.44
Yb	2.99	5.25	4.50	5.15	2.93	2.52	2.89	2.78
Lu	0.45	0.80	0.45	0.58	0.45	0.45	0.52	0.60
Ti	1072.62	476.72	1370.57	238.36	1549.34	1906.88	1310.98	2800.73
Normalised ratios								
Eu/Eu*	0.41	0.10	0.13	0.12	0.59	0.44	0.47	0.47
$(Nb/Zr)_N$[c]	9.02	2.09	5.07	5.57	2.54	3.84	7.55	8.15

[a] A/NK = $Al_2O_3/(Na_2O + K_2O)$ and A/CNK = $Al_2O_3/(CaO + Na_2O + K_2O)$, in moles

[b] FeOt = total iron expressed as FeO

[c] N = normalized to the values of McDonough and Sun [45]

Petrology	Amphibole-biotite granite				Biotite granite			
Sample	**Mak3**	**Mak4**	**Mak6**	**Mak7**	**Mak1**	**Mak2**	**Mak5**	**Mak9**
Major elements (wt%)								
$(Gd/Lu)_N$[c]	1.54	1.16	1.49	1.20	1.13	1.46	1.35	1.03
$(La/Yb)_N$[c]	14.53	3.28	4.09	4.35	6.42	8.12	6.55	6.06

[a] A/NK = $Al_2O_3/(Na_2O + K_2O)$ and A/CNK = $Al_2O_3/(CaO + Na_2O + K_2O)$, in moles

[b] FeOt = total iron expressed as FeO

[c] N = normalized to the values of McDonough and Sun [45]

Table 2
Whole-rock major (wt%) and trace-element (ppm) compositions of the gneisses and amphibolites of the Makassa area

Petrology	**Gneiss**		**Amphibolite**	
Sample	**Mak10**	**Mak11**	**Mak8**	**Mak12**
Major elements (wt%)				
SiO_2	60.87	62.82	58.33	53.83
TiO_2	0.93	0.82	0.89	1.07
Al_2O_3	15.10	14.75	17.44	15.66
Fe_2O_3	8.81	7.75	7.20	12.24
MgO	1.19	1.02	3.15	3.98
CaO	3.59	3.66	4.52	5.82
Na_2O	3.72	3.76	5.62	2.86
K_2O	4.81	5.26	2.26	4.24
MnO	0.01	0.01	0.11	0.06
P_2O_5	0.81	0.02	0.33	0.12
Sum	99.84	99.87	99.85	99.88
LOI	0.20	0.50	1.80	1.20
Ratios and indices				
A/NK[a]	1.33	1.24	1.49	1.68
A/CNK[a]	0.84	0.79	0.88	0.79
Na_2O+K_2O	8.53	9.02	7.88	7.10
Na_2O/K_2O	0.77	0.71	2.49	0.67
FeOt[b]	8.71	7.66	6.13	11.12

[a] A/NK = $Al_2O_3/(Na_2O + K_2O)$ and A/CNK = $Al_2O_3/(CaO + Na_2O + K_2O)$, in moles

[b] FeOt = total iron expressed as FeO

[c] N = normalized to the values of McDonough and Sun [45]

Petrology	**Gneiss**		**Amphibolite**	
Sample	**Mak10**	**Mak11**	**Mak8**	**Mak12**
Major elements (wt%)				
Rb/10	8.23	7.63	5.21	6.05
Ta×3	2.40	1.80	1.20	1.80
MgO/CaO	0.33	0.28	0.70	0.68
P_2O_5/TiO_2	0.87	0.93	0.71	0.52
Trace and rare earth elements (ppm)				
Cs	1.40	1.20	1.10	2.20
Rb	82.30	76.30	52.10	60.50
Ba	651.00	589.00	840.00	527.00
Sr	158.70	154.90	1071.00	998.30
Pb	2.50	3.50	1.40	1.90
Th	10.80	14.40	3.40	4.80
U	2.20	3.20	0.50	0.90
Zr	364.60	372.20	216.80	208.20
Hf	12.30	12.10	5.40	4.80
Ta	0.80	0.60	0.40	0.60
Y	45.60	42.80	20.60	22.20
Nb	28.70	26.70	10.10	12.40
Sc	4.00	4.00	11.00	10.00
Cr	18.00	20.00	14.00	12.00
Ni	19.00	20.00	38.00	28.00
Co	6.80	5.60	16.90	14.70
V	26.00	24.00	128.00	112.00

[a] A/NK = $Al_2O_3/(Na_2O + K_2O)$ and A/CNK = $Al_2O_3/(CaO + Na_2O + K_2O)$, in moles

[b] FeOt = total iron expressed as FeO

[c] N = normalized to the values of McDonough and Sun [45]

Petrology	**Gneiss**		**Amphibolite**	
Sample	**Mak10**	**Mak11**	**Mak8**	**Mak12**
Major elements (wt%)				
W	0.90	0.80	0.90	0.90
Ga	18.90	19.30	24.50	23.30
Zn	102.00	98.00	65.00	78.00
Cu	14.10	13.70	12.20	12.80
La	54.00	54.20	26.10	27.20
Ce	108.50	110.90	61.10	58.90
Pr	12.08	13.71	8.02	7.90
Nd	46.90	50.80	32.90	30.70
Sm	9.02	9.77	6.64	6.92
Eu	1.09	1.17	1.59	1.37
Gd	7.50	9.00	5.20	5.22
Tb	1.35	1.43	0.76	0.74
Dy	8.02	8.30	3.93	4.04
Ho	1.08	1.02	0.79	0.82
Er	4.28	4.54	2.23	3.07
Tm	0.63	0.61	0.32	0.44
Yb	3.89	3.97	1.99	2.02
Lu	0.56	0.52	0.31	0.42
Ti	5541.87	4886.38	5303.51	6376.13
Normalised ratios				
Eu/Eu*	0.40	0.38	0.83	0.70
$(Nb/Zr)_N$[c]	4.42	4.28	2.44	2.50

[a] A/NK = $Al_2O_3/(Na_2O + K_2O)$ and A/CNK = $Al_2O_3/(CaO + Na_2O + K_2O)$, in moles

[b] FeOt = total iron expressed as FeO

[c] N = normalized to the values of McDonough and Sun [45]

Petrology	Gneiss		Amphibolite	
Sample	**Mak10**	**Mak11**	**Mak8**	**Mak12**
Major elements (wt%)				
$(Gd/Lu)_N$[c]	1.66	2.14	2.07	1.54
$(La/Yb)_N$[c]	9.67	9.51	9.13	9.38
[a] A/NK = $Al_2O_3/(Na_2O + K_2O)$ and A/CNK = $Al_2O_3/(CaO + Na_2O + K_2O)$, in moles				
[b] FeOt = total iron expressed as FeO				
[c] N = normalized to the values of McDonough and Sun [45]				

4.2.1 General geochemical characteristics

The Makassa rock span 53.83–74.97 wt% SiO_2, 0.04–1.07% TiO_2, 12.94–17.44% Al_2O_3, 1.14–12.24% Fe_2O_3, 0.05–3.98% MgO, 0.82–5.82% CaO, 2.56–5.62% Na_2O, 2.26–5.26% K_2O, 0.01–0.25% MnO and 0.01–0.81% P_2O_5. The alkali sum ($Na_2O + K_2O$) ranges from 6.36 to 9.02 wt% and the Na_2O/K_2O ratio from 0.67 to 2.49. The trace-element contents vary widely: Ba 24–999 ppm, Sr 10.3–1071 ppm, Rb 52.1-243.7 ppm, Zr 109.2-381.7 ppm and Ti 238.36-6376.13 ppm.

4.2.2 Protolith of the metamorphic rocks

In the diagram of Werner [37] (Fig. 5), the gneiss plots in the field of ortho-derived rock and the amphibolite has a magmatic origin. Because their protoliths are magmatic, both rock types are treated together with the granitoids of the area in the following sections.

4.2.3 Classification and nomenclature

In the diagram of Cox *et al.* [38], adapted to plutonic rock by Wilson [39] (Fig. 6a), the samples plot in the granite and syeno-diorite fields, and all fall in the sub-alkaline domain. In the K_2O versus SiO_2 diagram of [40] (Fig. 6b), they occupy the calc-alkaline, high-K calc-alkaline and shoshonitic fields. In the FeOt/(FeOt + MgO) versus SiO_2 diagram of [41] (Fig. 6c), most samples are ferroan and only two are magnesian. In the A/NK versus A/CNK diagram of [42] (Fig. 6d), A/NK ranges from 1.14 to 1.68 and A/CNK from 0.79 to 1.17. Most samples are thus metaluminous I-type granitoids, whereas one granite sample is peraluminous and of S-type affinity (boundary after [43]).

4.2.4 Major-element variations

In the Harker diagrams (Fig. 7), Al_2O_3, Fe_2O_3, MgO, CaO and TiO_2 decrease with increasing SiO_2. Na_2O and K_2O vary little and show no correlation with SiO_2. P_2O_5 describes an arc-shaped trend.

4.2.5 Trace and rare earth elements

Harker diagrams of selected trace elements (Fig. 8) show scattered distributions of Ba, Rb, Nb, Zr and Ni with increasing silica, whereas V shows a linear trend for some samples.

The chondrite and primitive mantle normalized patterns (normalizing values of [45]; Fig. 9) are nearly parallel, sloping and serrated, with a marked enrichment in light rare earth elements (LREE) relative to heavy rare earth elements (HREE). The plutonic rocks (Fig. 9a) show strong fractionation [$(La/Yb)_N$ = 3.28–14.53], nearly flat HREE segments [$(Gd/Lu)_N$ = 1.03–1.54] and negative Eu anomalies (Eu/Eu* = 0.10–0.47). Their multi-element patterns (Fig. 9b) show negative Ba, Ta-Nb, Sr and Ti anomalies. The metamorphic rocks (Fig. 9c) are also strongly fractionated [$(La/Yb)_N$ = 9.13–9.67] with nearly flat HREE segments [$(Gd/Lu)_N$ = 1.54–2.14]. The gneiss has negative Eu anomalies (Eu/Eu* = 0.38–0.40), whereas the amphibolite has weak to no Eu anomaly (Eu/Eu* = 0.70–0.83). The multi-element patterns of the metamorphic rocks (Fig. 9d) show negative Ta-Nb, Ce, Zr and Ti anomalies and a positive Ba anomaly; the gneiss has a negative Sr anomaly, whereas the amphibolite has a positive one.

4.2.6 Tectonic discrimination

In the Rb versus (Y + Nb) diagram of [46] (Fig. 10a), all samples plot in the volcanic-arc and within-plate granite fields. In the Rb versus (Ta + Yb) diagram (Fig. 10b), they plot in the syn-collisional, volcanic-arc and within-plate granite fields.

5 Discussion

5.1 Petrogenetic evolution of the Makassa suite

The Makassa suite defines a continuous compositional array from 53.83 to 74.97 wt% SiO_2 that includes amphibole-biotite granite, biotite granite and the ortho-derived gneiss and amphibolite. The systematic decrease in Al_2O_3, Fe_2O_3, MgO, CaO and TiO_2 with increasing SiO_2 (Fig. 7) is consistent with progressive fractional crystallization of an amphibole + biotite + plagioclase + Fe-Ti oxide ± apatite assemblage from a common parental magma, rather than derivation of the granitoids and the meta-igneous rocks from unrelated sources. This interpretation is supported by the pronounced negative Eu, Ba, Sr and Ti anomalies of the granitoids (Eu/Eu* = 0.10–0.47), which reflect extensive plagioclase and Fe-Ti oxide fractionation, whereas the higher Sr and weak to absent Eu anomalies of the amphibolite (Eu/Eu* = 0.70–0.83) indicate a less evolved stage of the same magmatic system.

The compatible trace-element budget reinforces this fractionation-controlled scheme. Sc, V and Co decrease markedly from the amphibolite (V = 112–128 ppm; Co = 14.70–16.90 ppm) through the gneiss

to the granites (V = 9–32 ppm; Co = 0.20–5.60 ppm), tracking the progressive removal of amphibole and Fe-Ti oxides. Conversely, the incompatible elements Rb, Th and U increase with differentiation, whereas Ba and Sr decrease irregularly, consistent with concomitant K-feldspar and plagioclase fractionation. The arc-shaped P_2O_5-SiO_2 trend (Fig. 7) points to early apatite saturation followed by its removal once the melt became undersaturated in P_2O_5, a behaviour widely reported in evolved Pan-African calc-alkaline to high-K suites of Cameroon [47, 48].

Petrographic textures support this magmatic-differentiation scheme rather than a purely metamorphic or metasomatic origin for the granitoids. Simple Carlsbad twins in orthoclase, tartan-twinned microcline enclosing earlier biotite and quartz, and polysynthetic to albite-twinned plagioclase in the amphibolite and gneiss all indicate a magmatic crystallization sequence that was subsequently modified by localized subsolidus reactions (sericitization of plagioclase, chloritization of biotite and epidote formation after amphibole). Such reactions are typical of late- to post-magmatic deuteric alteration rather than pervasive regional metamorphism. The ortho-derived character of the gneiss and amphibolite (Fig. 5) is therefore consistent with their treatment as higher-temperature, less fractionated members of the same magmatic lineage as the granitoids, an approach also adopted for meta-igneous protoliths of comparable Pan-African massifs in Cameroon [49, 50].

Taken together, the geochemical and petrographic evidence supports a single-magma-source model in which the amphibolite and gneiss represent early, more mafic pulses, whereas the amphibole-biotite and biotite granites record progressively more differentiated liquids extracted from the same evolving reservoir. A continuum linked by fractional crystallization rather than by mixing of unrelated sources mirrors petrogenetic models proposed for other Pan-African plutonic complexes of the Adamawa-Yadé and North Cameroon domains, including the Batié and Misajé I-type massifs [48, 51] and the mafic-felsic associations of the Ngaoundal pluton [52].

5.2 Magma source and melting conditions

The Makassa granitoids are predominantly metaluminous, ferroan, high-K calc-alkaline to shoshonitic I-type rock with a single peraluminous S-type sample. Their LREE-enriched, HREE-flat patterns [$(La/Yb)_N$ up to 14.53; $(Gd/Lu)_N$ = 1.03–1.54], combined with marked Nb-Ta, Ba, Sr and Ti depletion, are typical of magmas derived from partial melting of a pre-enriched, amphibole- and/or biotite-bearing infracrustal source (tonalitic-granodioritic lower to middle crust). A contribution from mantle-derived melts is possible and is suggested by the two magnesian samples.

The nearly flat HREE segments of both the granitoids and the amphibolite [$(Gd/Lu)_N$ = 1.03–2.14] indicate that garnet was not a significant residual phase, which points to a shallow, plagioclase-stable, garnet-absent source rather than a deep eclogitic or garnet-amphibolite protolith. This is consistent with the negative Sr and Eu anomalies of the granitoids, which reflect plagioclase retention in the residue or its removal by fractional crystallization, whereas the positive Sr anomaly and weak Eu anomaly of the amphibolite suggest a plagioclase-poor, less fractionated melt closer to the parental composition. The strong Nb-Ta depletion relative to Th and La in all lithologies further points to a source previously

modified by subduction-related fluids or melts, a signature that is inherited rather than newly acquired during post-collisional melting [53].

The ferroan character of most samples, together with their high-K to shoshonitic affinities, implies relatively reduced, dry to moderately hydrous melting conditions and elevated magmatic temperatures. These features are consistent with anatexis of a previously dehydrated, biotite ± amphibole-bearing crustal source rather than low-temperature, water-saturated, fluid-fluxed melting. The coexistence of one peraluminous S-type sample with a dominantly metaluminous I-type population suggests the local incorporation of a metasedimentary (pelitic) component, either by partial melting of interlayered metasediments or by minor crustal contamination during magma ascent. A hybrid I-/S-type relationship of this kind has also been documented in the Bafoussam complex, where both suites were attributed to a common infracrustal source variably contaminated by supracrustal material [47].

This dual signature, dominantly crustal but locally mantle-influenced, parallels the hybrid mantle-crust models proposed for the I and S-type granitoids of the Bafoussam complex [47] and for the high-K I-type granites of the Batié and Misajé plutons [48, 51], where crustal reworking is accompanied by minor mafic input from a metasomatized lithospheric mantle. The ferropotassic, high-K character of the Makassa rocks also has analogues in the post-collisional granitoids of the Nigerian sector of the belt [53], suggesting a regionally consistent thermal and compositional regime for late-orogenic melting along this segment of the CAFB.

5.3 Geodynamic significance: from arc to post-collisional magmatism

The overlap of the Makassa samples between the volcanic-arc (VAG) and within-plate (WPG) granite fields in Fig. 10a, and between the syn-collisional (syn-COLG), VAG and WPG fields in Fig. 10b, does not indicate a genuinely ambiguous tectonic setting. It is a well-recognized geochemical signature of post-collisional granitoids, whose trace-element budget inherits the arc-like imprint of a previously subduction-modified crustal or mantle source while the magmas are emplaced in an extensional to transtensional, no-longer-convergent regime [48, 54].

This field overlap is widely recognized as a limitation of discrimination diagrams calibrated on modern convergent settings when they are applied to post-collisional granitoids, whose parental magmas are generated by decompression melting of a lithospheric mantle and lower crust that were metasomatized during an earlier subduction stage [55]. The high-K calc-alkaline to shoshonitic affinity of the Makassa rocks, together with their ferroan character and Nb-Ta-Ti depletion, is consistent with melting triggered by lithospheric thinning or delamination following crustal thickening, rather than with active subduction-related magma generation. A similar mechanism has been invoked for the synkinematic Bocaranga plutonic complex, emplaced along the Mbéré Shear Zone during the late- to post-collisional D2 deformation phase of the Adamawa-Yadé Domain [55].

In this framework, the Makassa magmatism is best interpreted as recording the transition from a late collisional to a post-collisional stage of the Pan-African orogeny. It is broadly comparable to the high-K I-type Batié massif, emplaced along the Kékem-Fotouni shear zone, which is the southwestern extension of the Tcholliré-Banyo Fault [48], and to the collisional to post-collisional granitic suites of the Guéra Massif in south-central Chad, which record a similar shift in geochemical affinity over a short time interval during the terminal stages of the orogeny [54]. The association of the Makassa granitoids with the Rey Bouba greenstone belt and their proximity to the Tcholliré-Banyo shear zone further support emplacement along a crustal-scale structure that accommodated the switch from collisional shortening to transcurrent, extension-assisted magma ascent.

The geochemical signature of the Makassa suite is therefore not anomalous but fits a recurrent pattern along the CAFB, in which shear-zone-controlled, high-K to shoshonitic post-collisional magmatism developed diachronously but mechanistically consistently from Nigeria through Cameroon to Chad and the Central African Republic [48, 53–55], marking the terminal, extensional readjustment of the belt after continental collision.

5.4 Regional implications within the Pan-African Fold Belt

The Makassa magmatism fits within a broader pattern of late- to post-collisional, high-K calc-alkaline to shoshonitic plutonism that characterizes the northern and central sectors of the CAFB, from the Adamawa-Yadé Domain [47, 48, 51] to its extensions in the Central African Republic [55] and Chad [54, 56]. The recurrence of a similar magmatic style across such a wide segment of the belt argues for a shared, orogen-scale mechanism of lithospheric thinning and shear-zone-controlled melting during the terminal stages of the orogeny, rather than for isolated, locally driven magmatic episodes restricted to individual massifs.

Within the Mayo-Kébbi/North Cameroon arc itself, the only radiometric constraints remain the Rb/Sr whole-rock ages of 626 ± 15 Ma and 677 ± 40 Ma obtained by [28] on the deformed Kaélé granites. The geochemical affinities documented here for Makassa, together with the Nb-Ta-mineralized, late-Neoproterozoic (603 – 582 Ma) Mayo Salah leucogranite further west in the North Cameroon domain [57], suggest that magmatism along this arc may have continued, or been reactivated, well into the terminal, post-collisional stages of the Pan-African orogeny (ca. 610 – 540 Ma), as elsewhere along the belt. If confirmed, this diachroneity would place the Mayo-Kébbi/North Cameroon arc among the longer-lived magmatic segments of the CAFB, bridging the early collisional ages inherited from Lasserre's dataset with the younger post-collisional pulses documented from Nigeria to Chad. New U-Pb geochronological data on the Makassa granitoids are needed to test this correlation and to place this segment of the Mayo-Kébbi Domain more precisely within the regional tectono-magmatic chronology of the CAFB.

6 Conclusions

Petrographic and geochemical investigation of 12 representative samples from the Makassa area, located within the North Cameroon Domain of the Central African Fold Belt (CAFB), indicates that the Makassa suite is compositionally continuous, with SiO_2 contents ranging from 53.83 to 74.97 wt%, and comprises amphibole-biotite granite, biotite granite, ortho-derived gneiss and amphibolite. The systematic decrease in Al_2O_3, Fe_2O_3, MgO, CaO and TiO_2 with increasing SiO_2, together with pronounced negative Eu, Ba, Sr and Ti anomalies, suggests that these lithologies are cogenetic and resulted from fractional crystallization of an amphibole + biotite + plagioclase + Fe-Ti oxide ± apatite assemblage from a common parental magma. The rocks are predominantly metaluminous to weakly peraluminous, ferroan, high-K calc-alkaline to shoshonitic I-type granitoids, with A/CNK values ranging from 0.79 to 1.17, except for a single peraluminous S-type sample. Their enrichment in LREE, relatively flat HREE patterns, and marked depletion in Nb-Ta, Ba, Sr and Ti indicate a dominantly crustal source, most plausibly involving partial melting of a pre-enriched infracrustal tonalitic–granodioritic protolith, with a possible minor mantle contribution suggested by two magnesian samples. Tectonic discrimination diagrams place the samples within overlapping volcanic-arc, syn-collisional and within-plate granite fields, a geochemical signature interpreted as characteristic of a post-collisional setting that inherited an arc-related source. The Makassa magmatism therefore appears to record the transition from late-collisional to post-collisional tectonic conditions during the Pan-African orogeny, consistent with similar magmatic transitions documented along the Tcholliré-Banyo Fault system and elsewhere in the Adamawa-Yadé Domain, the Central African Republic and Chad. These findings provide the first quantitative geochemical characterization of Pan-African magmatism in the Far North Cameroon sector of the Mayo-Kébbi/North Cameroon arc, which was previously constrained mainly by Rb-Sr geochronological data from the Kaélé granites. The geochemical affinity of the Makassa rock with late- to post-collisional plutonic suites dated at approximately 610 – 540 Ma elsewhere in the Central African Fold Belt suggests that magmatic activity within this arc may have persisted or been reactivated during the terminal stages of the Pan-African orogeny. However, in the absence of direct geochronological data for the Makassa rock, this regional correlation remains provisional. U-Pb zircon geochronology combined with Sr-Nd isotopic analyses is therefore recommended to establish the precise temporal position of the Makassa magmatism within the regional evolution of the CAFB and to further constrain the relative contributions of crustal and mantle sources inferred from the present geochemical data.

Declarations

Acknowledgements

The authors thank the Geological and Mining Research Institute (IRGM, Yaoundé) for the preparation of the thin sections and the Mines and Geology Laboratory of the University of Ngaoundéré for access to microscopy facilities.

Author contributions

Conceptualization, methodology, investigation, writing - original draft : Amadou Diguim Kepnamou. Formal analysis and visualization : Amadou Diguim Kepnamou and Naïmou Seguem. Supervision : Ganwa Alembert Alexandre and Ngounouno Ismaïla. All authors reviewed and approved the final manuscript.

Funding

The authors received no specific funding for this work.

Data availability

All data generated or analysed during this study are included in this published article (Tables 1 and 2).

Ethics approval and consent to participate

Not applicable.

Consent for publication

Not applicable.

Competing interests

The authors declare no competing interests.

References

1. Lasserre M, Soba D. Age libérien des granodiorites et des gneiss à pyroxènes du Cameroun méridional. Bull BRGM, 2ème série, section IV. 1979;(2):17–32.
2. Bessoles B, Trompette R. La chaîne pan-africaine et son avant pays au Cameroun, en République Centrafricaine et au Tchad. Géologie de l'Afrique: la chaîne panafricaine « zone mobile d'Afrique centrale » (partie Sud) et « zone mobile soudanaise ». Volume 92. Orléans: BRGM; 1980. (Mémoires du BRGM.
3. Affaton P, Sougy J, Trompette R. The tectonic environment of the Buem volcanic-sedimentary formation and the Pan-African Dahomeyide orogeny, West Africa. Precambrian Res. 1991;49:47–58.
4. Nzenti JP. Pétrogenèse des migmatites de Yaoundé (Cameroun): éléments pour un modèle géodynamique de la chaîne panafricaine Nord-Equatoriale [doctoral thesis]. Nancy: Université de Nancy I; 1987.
5. Poidevin JL. La géologie de la République Centrafricaine, chaîne panafricaine et craton congolais. Notice explicative de la carte géologique au 1/1 500 000. Orléans: BRGM; 1983. (Bulletin du BRGM).
6. Ngako V, Jégouzo P, Nzenti JP. Le cisaillement centre camerounais: rôle structural et géodynamique dans l'orogenèse panafricaine. C R Acad Sci Paris. 1992;315:457–63.

7. Ngako V, Affaton P, Nnange JM, Njanko T. Pan-African tectonic evolution in central and southern Cameroon: transpression and transtension during sinistral shear movements. J Afr Earth Sci. 2003;36:207–14.
8. Castaing C, Triboulet C, Feybesse JL, Chèvremont P. Tectonometamorphic evolution of Ghana, Togo and Benin in the light of the Pan-African/Brasiliano orogeny. Tectonophysics. 1994;218:323–42.
9. Abdelsalam MG, Liégeois JP, Stern RJ. The Saharan Metacraton. J Afr Earth Sci. 2002;34:119–36.
10. Liégeois JP, Latouche L, Boughrara M, Navez J, Guiraud M. The LATEA metacraton (Central Hoggar, Tuareg Shield, Algeria): behaviour of an old passive margin during the Pan-African orogeny. J Afr Earth Sci. 2003;37:161–90.
11. Liégeois JP, Abdelsalam MG, Ennih N, Ouabadi A. Metacraton: nature, genesis and behavior. Gondwana Res. 2013;23:220–37.
12. Oliveira EP, Windley BF, Araújo MNC. The Neoproterozoic Sergipano orogenic belt, NE Brazil: a complete plate tectonic cycle in Western Gondwana. Precambrian Res. 2006;151:1–35.
13. Ngako V, Njonfang E, Aka FT, Affaton P, Metuk Nyada R. Extensional tectonics in the Pan-African Yaoundé Belt, Cameroon: evidence from Bissaula-Bali Fault Zone and bordering granulitic rock. J Afr Earth Sci. 2008;44:494–502.
14. Almeida FFM, Hasui Y, Brito Neves BB, Fuck RA. Brazilian structural provinces: an introduction. Earth-Sci Rev. 1981;17:1–29.
15. Castaing C, Feybesse JL, Thiéblemont D, Triboulet C, Chèvremont P. Paleogeographical reconstructions of the Pan-African/Brasiliano orogen: closure of an oceanic domain or intracontinental convergence between major blocks? Precambrian Res. 1993;69:327–44.
16. Neves SP, Bruguier O, Vauchez A, Bosch D, Silva JMR, Mariano G. Zircon U-Pb geochronology of the Borborema Province, NE Brazil: SHRIMP and conventional data and their bearing on interpretation of crustal evolution. J South Am Earth Sci. 2004;17:87–101.
17. Van Schmus WR, Oliveira EP, Da Silva Filho AF, Toteu SF, Penaye J, Guimarães IP. Proterozoic links between the Borborema Province, NE Brazil, and the Central African Fold Belt. In: Pankhurst RJ, Trouw RAJ, De Brito Neves BB, De Wit MJ, editors. West Gondwana: pre-Cenozoic correlations across the South Atlantic region. Volume 294. London: Geological Society; 2008. pp. 69–99.
18. Archanjo CJ, Viegas LGF, Hollanda MHBM, Souza LC, Liu D. Timing of the HT/LP transpression in the Neoproterozoic Seridó Belt (Borborema Province, Brazil): constraints from U-Pb (SHRIMP) geochronology and implications for the connections between NE Brazil and West Africa. Gondwana Res. 2013;23:701–14.
19. Toteu SF, Penaye J, Poudjom Djomani Y. Geodynamic evolution of the Pan-African belt in central Africa with special reference to Cameroon. Can J Earth Sci. 2004;41:73–85.
20. Penaye J, Kröner A, Toteu SF, Van Schmus WR, Doumnang JC. Evolution of the Mayo Kebbi region as revealed by zircon dating: an early (ca. 740 Ma) Pan-African magmatic arc in southwestern Chad. J Afr Earth Sci. 2006;44:530–42.

21. Liégeois JP, Black R, Navez J, Latouche L. Early and late Pan-African orogenies in the Aïr assembly of terranes (Tuareg Shield, Niger). Precambrian Res. 1993;87:93–118.
22. Ngako V. Structures et évolution tectonique du domaine panafricain nord de la chaîne panafricaine au Cameroun [Thèse de Doctorat d'Etat]. Yaoundé: Université de Yaoundé I; 1999.
23. Ngako V, Njonfang E. Plates amalgamation and plate destruction, the Western Gondwana history. In: Ali D, editor. Tectonics – recent advances. Rijeka: InTech; 2011. pp. 3–30.
24. Caby R, Bertrand JML, Black R. Pan-African ocean closure and continental collision in the Hoggar-Iforas segment, central Sahara. In: Kröner A, editor. Precambrian plate tectonics. Amsterdam: Elsevier; 1981. pp. 407–34.
25. Black R, Latouche L, Liégeois JP, Caby R, Bertrand JM. Pan-African displaced terranes in the Tuareg Shield (central Sahara). Geology. 1994;22:641–4.
26. Louis P. Contribution géophysique à la connaissance géologique du bassin du lac Tchad. Volume 42. Paris: ORSTOM; 1970. (Mémoires ORSTOM.
27. Freeth SJ. Envisaged Eburnian/Pan-African suture zones in Nigeria and Cameroon. J Afr Earth Sci. 1984;2:81–3.
28. Lasserre M. Nouvelles données géochronologiques sur les granites de la zone mobile de l'Afrique Centrale au Cameroun. C R Acad Sci Paris. 1967;264:2926–9.
29. Toteu SF. Geochemical characterization of the main petrographical and structural units of northern Cameroon: implications for Pan-African evolution. J Afr Earth Sci. 1990;10:615–26.
30. Doumnang JC. Etude structurale, métallogénique et géochimique des ceintures de roches vertes de Pala et Melfi (Sud-Ouest du Tchad): un exemple de croûte juvénile néoprotérozoïque accrétée au continent Ouest Africain [doctoral thesis]. Dijon: Université de Bourgogne; 2006.
31. Isseini M. Etude pétro-structurale, géochimique et géochronologique du massif de Guéra (Tchad): un exemple de croûte continentale néoprotérozoïque en Afrique Centrale [doctoral thesis]. Nancy: Université Henri Poincaré; 2011.
32. Bouyo Houketchang M, Zhao Y, Penaye J, Zhang SH, Njel UO. Neoproterozoic subduction-related metavolcanic and metasedimentary rock from the Rey Bouba Greenstone Belt of north-central Cameroon in the Central African Fold Belt: new insights into a continental arc geodynamic setting. Precambrian Res. 2015;261:40–53.
33. Toteu SF, Van Schmus WR, Penaye J, Michard A. New U-Pb and Sm-Nd data from north-central Cameroon and its bearing on the pre-Pan-African history of Central Africa. Precambrian Res. 2001;108:45–73.
34. Pouclet A, Doumnang JC, Vidal M, Delor C, Peucat JJ. Neoproterozoic crust formation in southwestern Chad: geochemical and Sr-Nd isotopic evidence for the correlation with the Central African Belt. J Afr Earth Sci. 2006;44:543–60.
35. Penaye J. Métamorphisme et évolution tectonique de la partie orientale de la chaîne panafricaine au Cameroun [Thèse de Doctorat 3ème cycle]. Nancy: Université de Nancy I; 1988.

36. Toteu SF, Michard A, Bertrand JM, Rocci G. U/Pb dating of Precambrian rock from northern Cameroon, orogenic evolution and chronology of the Pan-African belt of Central Africa. Precambrian Res. 1987;37:71–87.
37. Werner CD. Saxonian granulites: a contribution to the geochemical diagnosis of original rocks in high-metamorphic complexes. Gerlands Beitr Geophys. 1987;96:271–90.
38. Cox KG, Bell JD, Pankhurst RJ. The interpretation of igneous rocks. London: George Allen & Unwin; 1979.
39. Wilson M. Igneous petrogenesis: a global tectonic approach. London: Unwin Hyman; 1989.
40. Le Maître RW, Bateman P, Dudek A, Keller J, Le Lameyre MJ, Sabine PA, et al. A classification of igneous rocks and glossary of terms: recommendations of the International Union of Geological Sciences Subcommission on the Systematics of Igneous Rocks. Oxford: Blackwell Scientific; 1989.
41. Frost BR, Barnes CG, Collins WJ, Arculus RJ, Ellis DJ, Frost CD. A geochemical classification for granitic rock. J Petrol. 2001;42:2033–48.
42. Maniar PD, Piccoli PM. Tectonic discrimination of granitoids. Geol Soc Am Bull. 1989;101:635–43.
43. Chappell BW, White AJR. I- and S-type granites in the Lachlan Fold Belt. Trans R Soc Edinb Earth Sci. 1992;83:1–26.
44. Irvine TN, Baragar WRA. A guide to the chemical classification of the common volcanic rocks. Can J Earth Sci. 1971;8:523–48.
45. McDonough WF, Sun SS. The composition of the Earth. Chem Geol. 1995;120:223–53.
46. Pearce JA, Harris NBW, Tindle AG. Trace element discrimination diagrams for the tectonic interpretation of granitic rock. J Petrol. 1984;25:956–83.
47. Djouka-Fonkwé ML, Schulz B, Schüssler U, Tchouankoué JP, Nzolang C. Geochemistry of the Bafoussam Pan-African I- and S-type granitoids in western Cameroon. J Afr Earth Sci. 2008;50:148–67.
48. Kwékam M, Talla V, Fozing EM, Tcheumenak Kouémo J, Dunkl I, Njonfang E. The Pan-African high-K I-type granites from Batié Complex, West Cameroon: age, origin, and tectonic implications. Front Earth Sci. 2020;8:363.
49. Nsifa Nkonguin E, Tchameni R, Nédélec A, Siqueira R, Pouclet A, Bascou J. Structure and petrology of Pan-African nepheline syenites from South West Cameroon; implications for their emplacement mode, petrogenesis and geodynamic significance. J Afr Earth Sci. 2013;87:44–58.
50. Messi Ottou EJ, Ntomba SM, Ntieche B, Magnekou Takamte RC, Bisse SB, Ndong Bidzang F, et al. Petrology of the meta-mafic rock from the Lolodorf area, Nyong Complex (Southwest Cameroon): implication for the origin and emplacement conditions. SN Appl Sci. 2022;4:293.
51. Fozing EM, Kwékam M, Tetsopgang S, Njanko T, Chako-Tchamabé B, Tcheumenak Kouémo J, et al. The mineralization potential of the I-type granites from Misajé pluton (NW-Cameroon): AMS and geochemical constraints. Solid Earth Sci. 2021;6:283–96.

52. Mamouda A, Ganno S, Tchoupe Takam Bertin G, Mbita Motto Steven A, Fossi HD, Nzenti JP, et al. Origin and intraplate tectonic setting of mafic magmatic enclaves from the Ngaoundal area, Adamawa-Cameroon: insights from petrography and geochemistry. China Geol. 2022;5:579–94.
53. Ferré EC, Gleizes G, Caby R. Obliquely convergent tectonics and granite emplacement in the Trans-Saharan Belt of eastern Nigeria: a synthesis. Precambrian Res. 2002;114:199–219.
54. Pham CT, Shellnutt JG, Yeh MW, Iizuka Y. An assessment of the magmatic conditions of Late Neoproterozoic collisional and post-collisional granites from the Guéra Massif, south-central Chad. Front Earth Sci. 2020;8:318.
55. Topien RM, Tcheumenak Kouémo J, Kpéou J, Moloto-A-Kenguemba G, Kwékam M. Petrology of the Pan-African high-K alkali-calcic Bocaranga plutonic complex in the Adamawa-Yadé Domain (Central African Republic): nature, origin and contribution to geodynamic reconstruction of the Central African Fold Belt. Solid Earth Sci. 2024;9:100211.
56. Djerossem F, Berger J, Vanderhaeghe O, Isseini M, Ganne J, Zeh A. Neoproterozoic magmatic evolution of the southern Ouaddaï Massif (Chad). BSGF Earth Sci Bull. 2020;191:34.
57. Fosso Tchunte PM, Tchouankoue JP, Bybee GM, Nzepang Tankwa M, Simeni Wambo NA, Ganno S. Evidence for Nb-Ta occurrences in the syn-tectonic Pan-African Mayo Salah leucogranite (northern Cameroon): constraints from Nb-Ta oxide mineralogy, geochemistry and U-Pb LA-ICP-MS geochronology on columbite and monazite. Minerals. 2018;8:190.

Figures

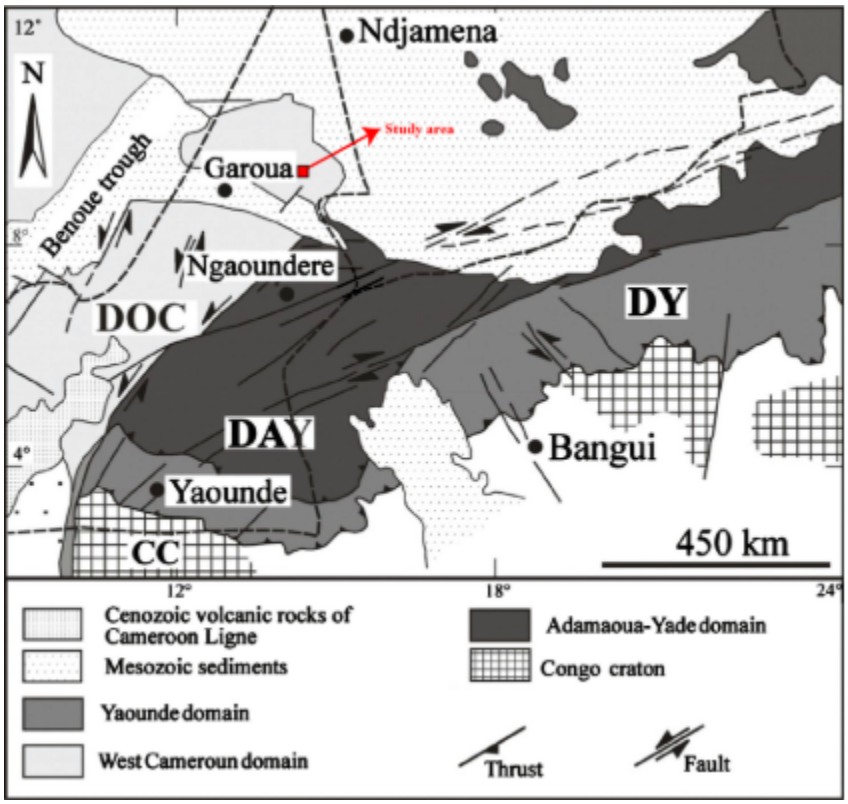


Figure 1

Geological sketch map of the Pan-African belt north of the Congo Craton showing the study area (modified after [19]). DOC, Far North Cameroon Domain; DAY, Adamawa-Yadé Domain; DY, Yaoundé Domain; CC, Congo Craton

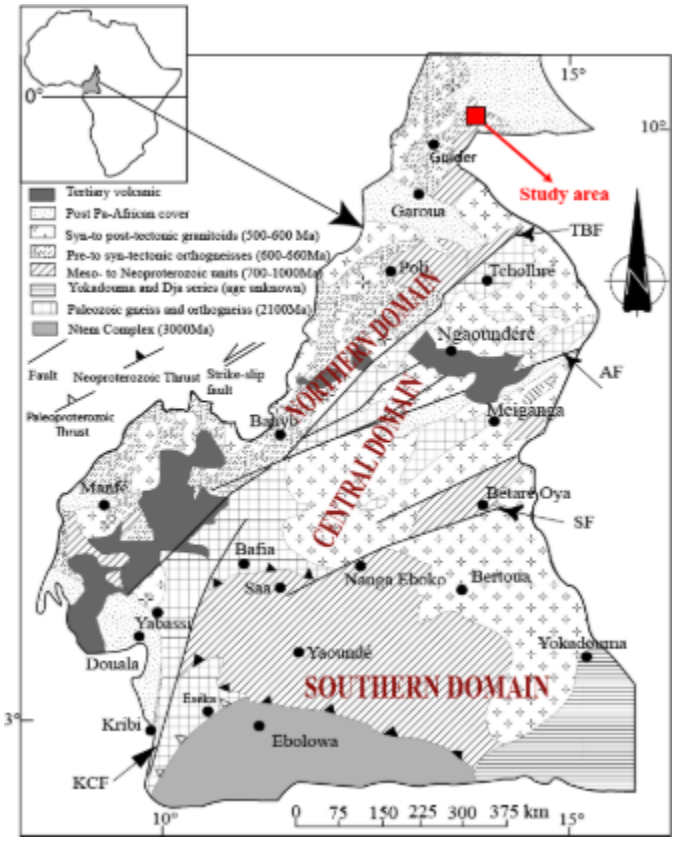


Figure 2

Geological map of the Pan-African Fold Belt (PAFB) north of the Congo Craton showing the study area (simplified after [19])

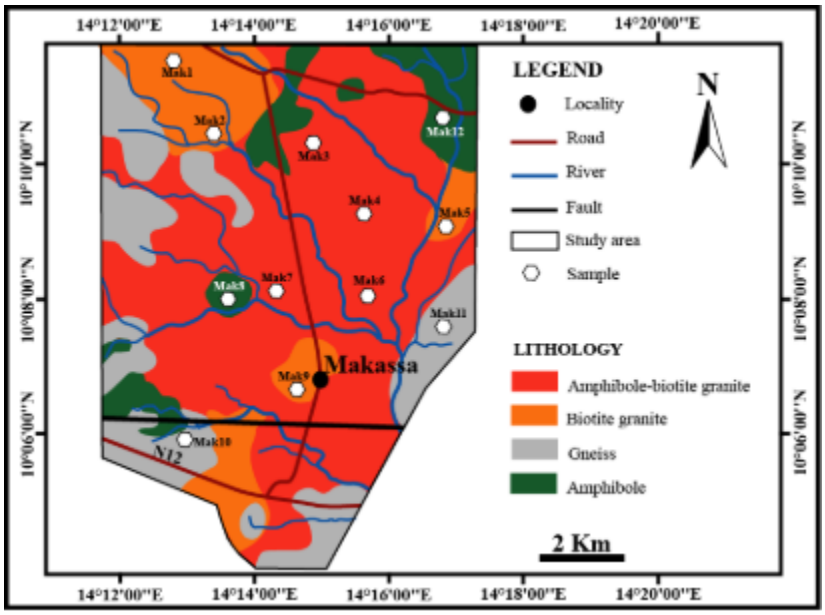


Figure 3

Geological outcrop map of the Makassa area showing the main rock types identified through field and petrographic investigations

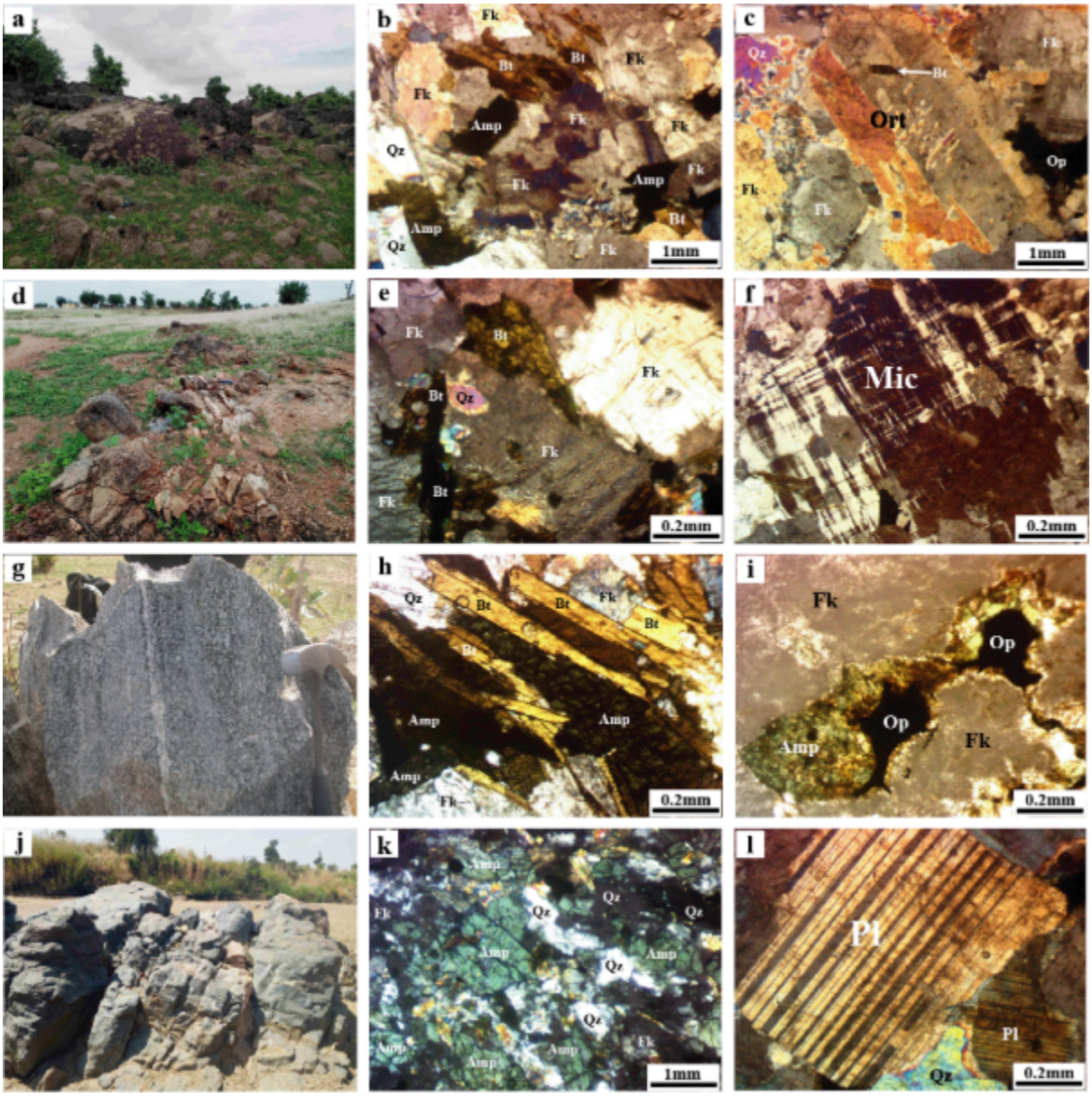


Figure 4

Outcrops and thin-section photomicrographs of the Makassa rocks. a Slab and block outcrop of amphibole-biotite granite; b granular texture of amphibole-biotite granite (XPL); c orthoclase with Carlsbad twinning (XPL); d block outcrop of biotite granite; e granular texture of biotite granite (XPL); f microcline with inclusions of biotite and opaque minerals (XPL); g schistose structure of the gneiss outcrop; h amphibole–biotite association illustrating the lepidoblastic texture of the gneiss (XPL); i association of amphibole and opaque minerals (PPL); j amphibolite outcrop in the streambed; k granoblastic texture of amphibolite (XPL); l plagioclase with albite twinning (XPL). PPL, plane-polarized light; XPL, cross-polarized light

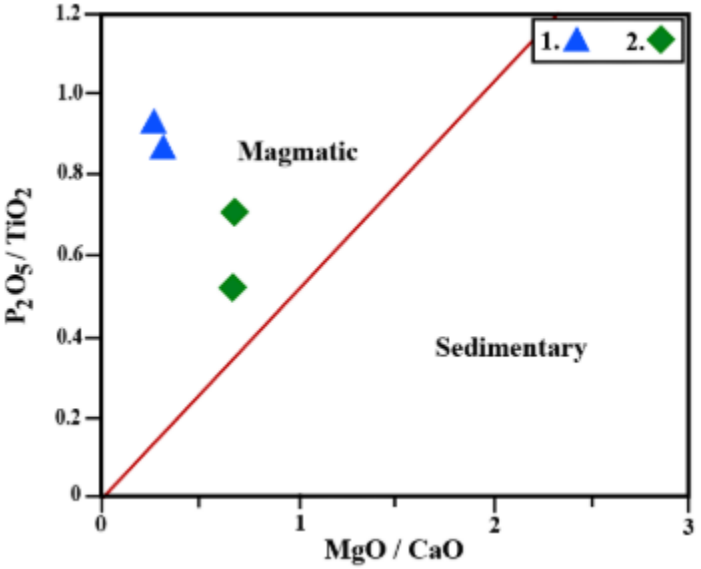


Figure 5

Determination of the protolith nature of the metamorphic rocks of the Makassa area using the diagram of Werner [37].

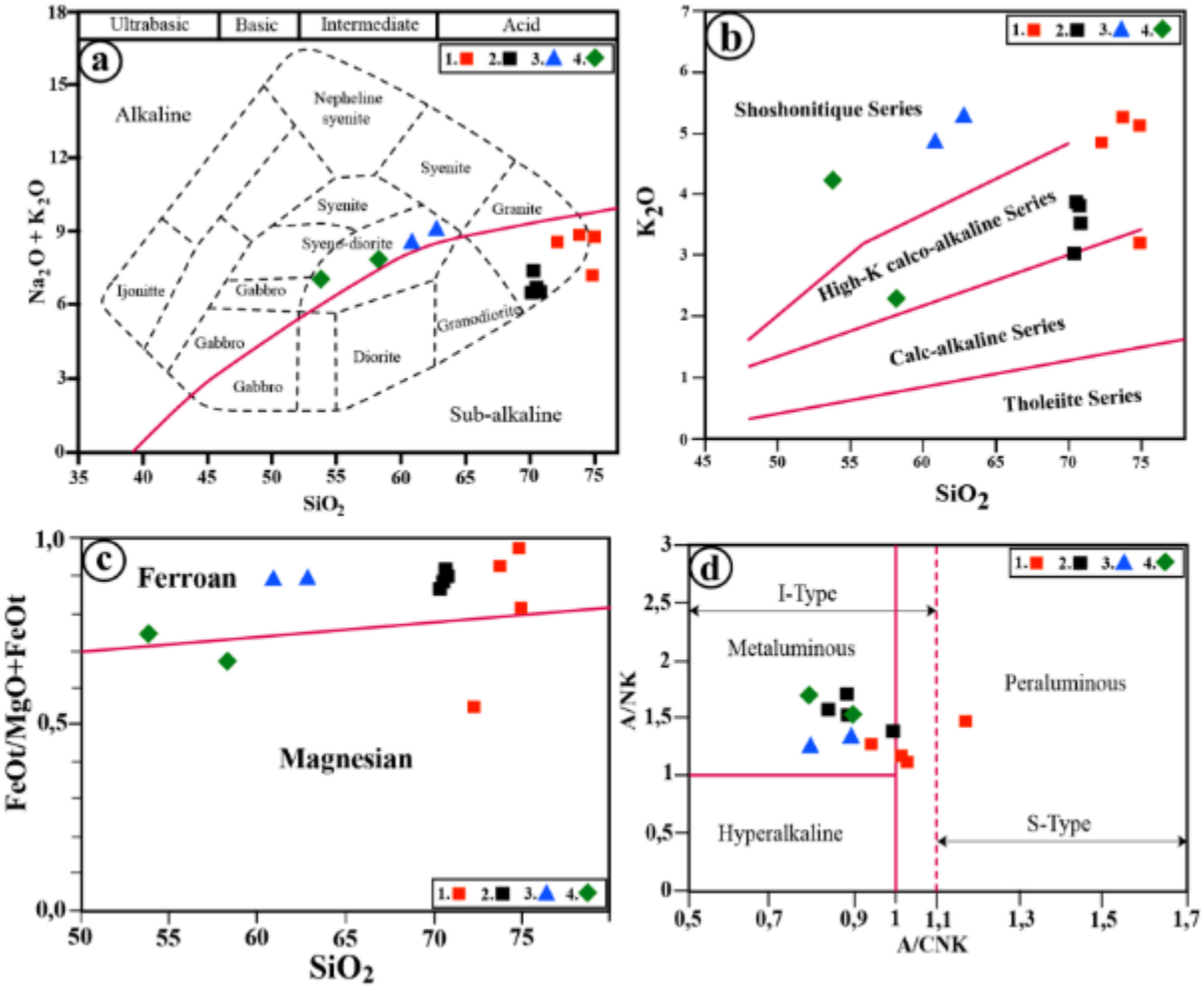


Figure 6

Classification of the Makassa rock. **a.** Diagram of Cox *et al.* [38] adapted to plutonic rocks by Wilson [39]; the bold line separates the alkaline and sub-alkaline fields [44]. **b.** K_2O versus SiO_2 diagram; series boundaries from [40]. **c.** FeOt/(MgO + FeOt) versus SiO_2 diagram of [41] showing the ferroan and magnesian fields. **d.** A/NK versus A/CNK diagram of [42]; A/NK = $Al_2O_3/(Na_2O + K_2O)$ and A/CNK = $Al_2O_3/(CaO + Na_2O + K_2O)$ in moles; the I- and S-type boundary is from [43]. **1.** Amphibole-biotite granite; **2.** Biotite granite; **3.** Gneiss; **4.** Amphibolite.

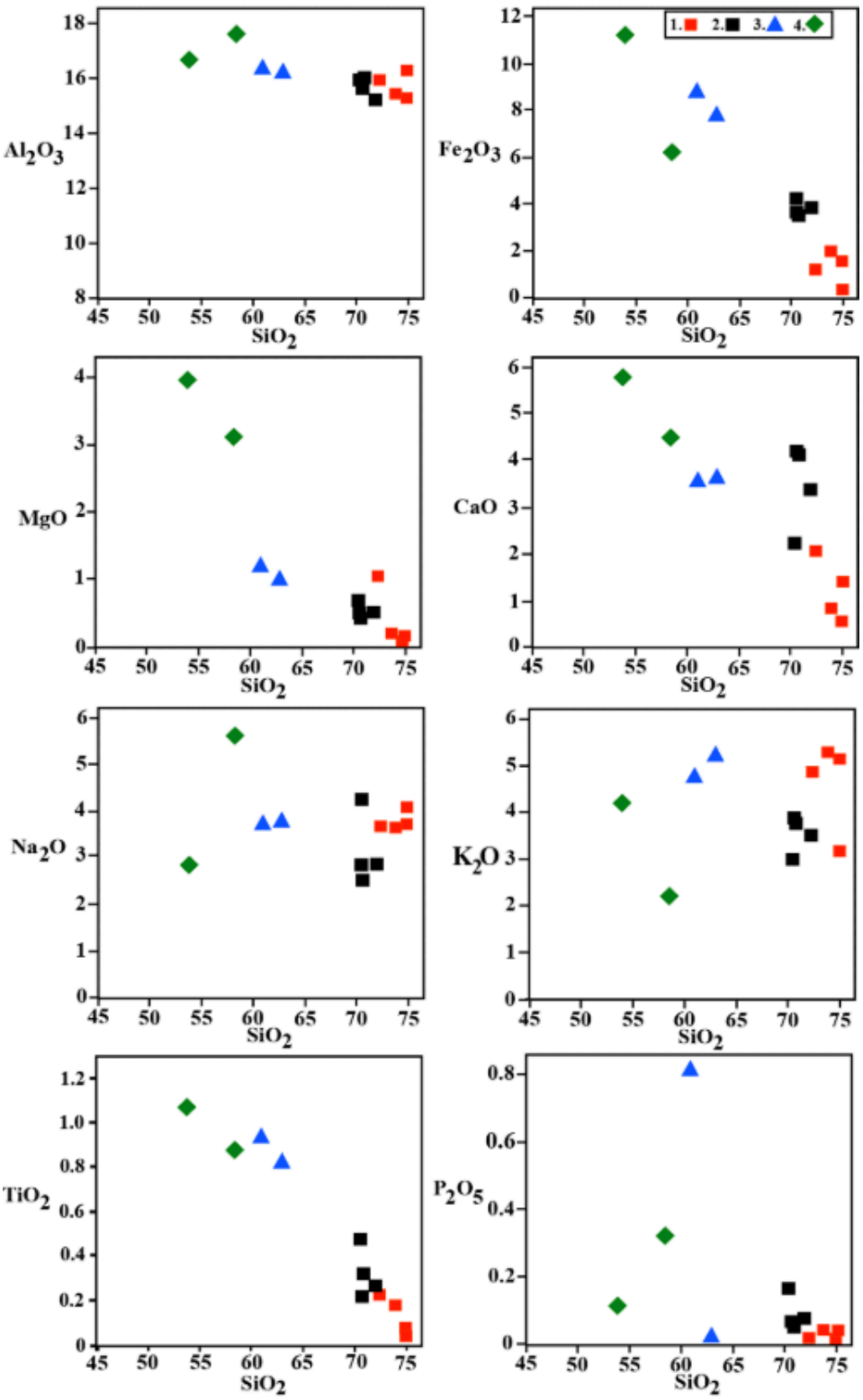


Figure 7

Harker diagrams of major oxides versus SiO_2 for the Makassa rock. **1.** Amphibole-biotite granite; **2.** Biotite granite; **3.** Gneiss; **4.** Amphibolite.

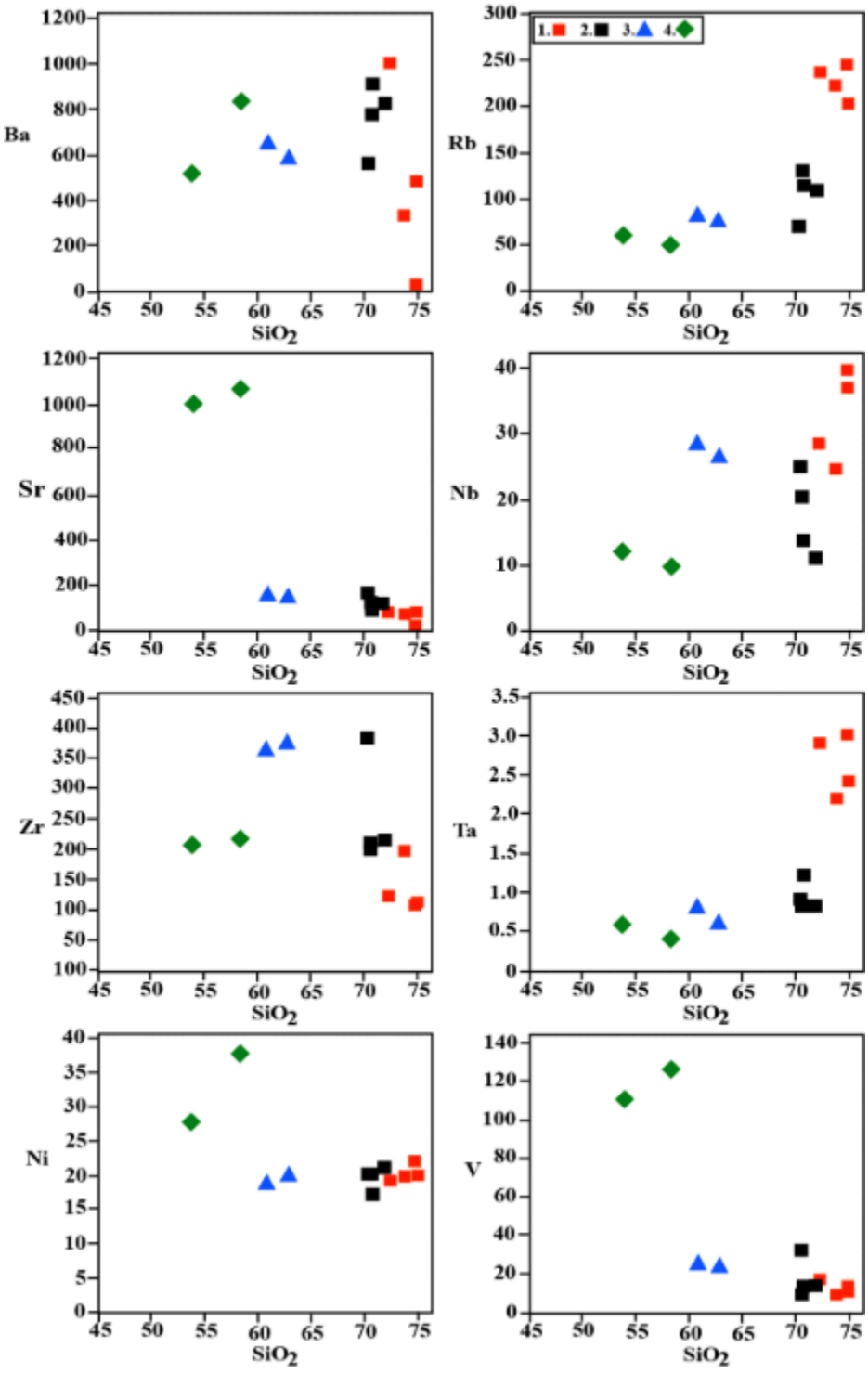


Figure 8

Harker diagrams of selected trace elements versus SiO_2 for the Makassa rock. **1.** Amphibole-biotite granite; **2.** Biotite granite; **3.** Gneiss; **4.** Amphibolite.

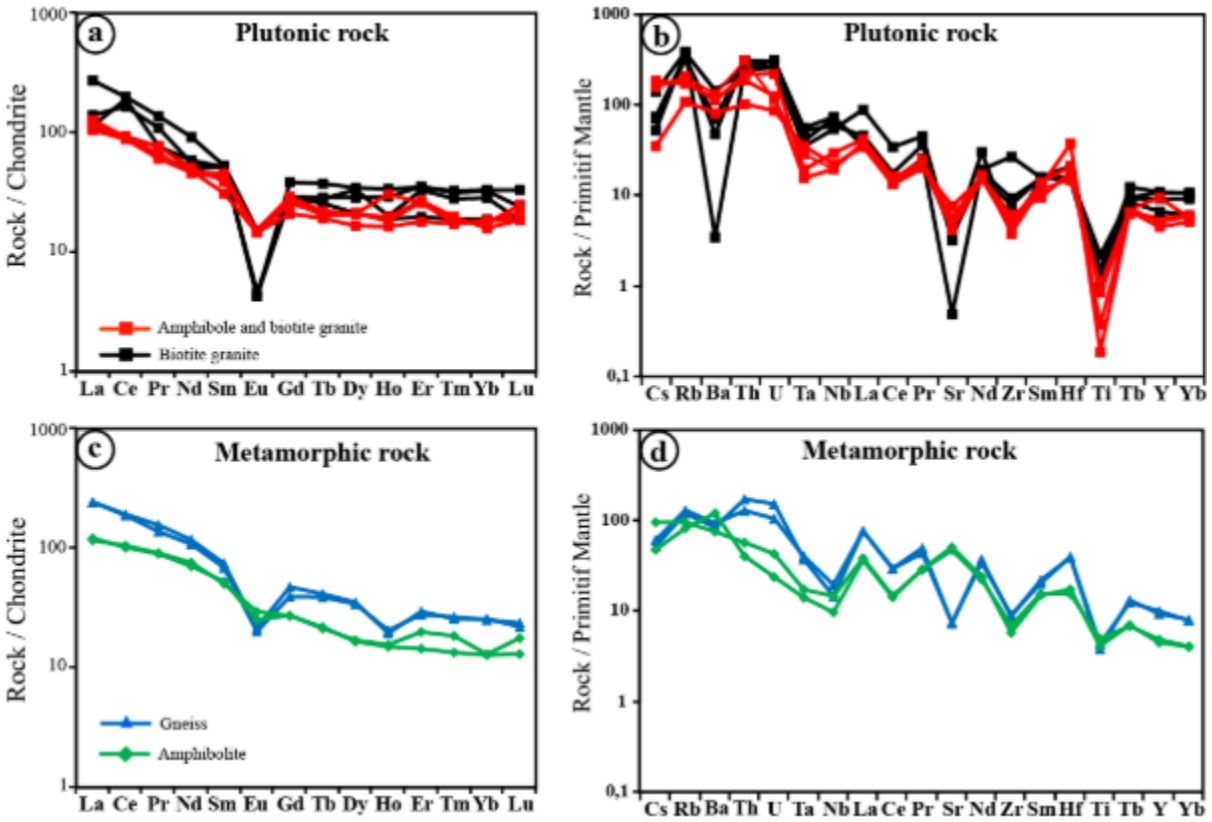


Figure 9

Rare earth element patterns **(a, c)** and multi-element patterns **(b, d)** of the plutonic **(a, b)** and metamorphic **(c, d)** rocks of the Makassa area, normalized to the values of [45].

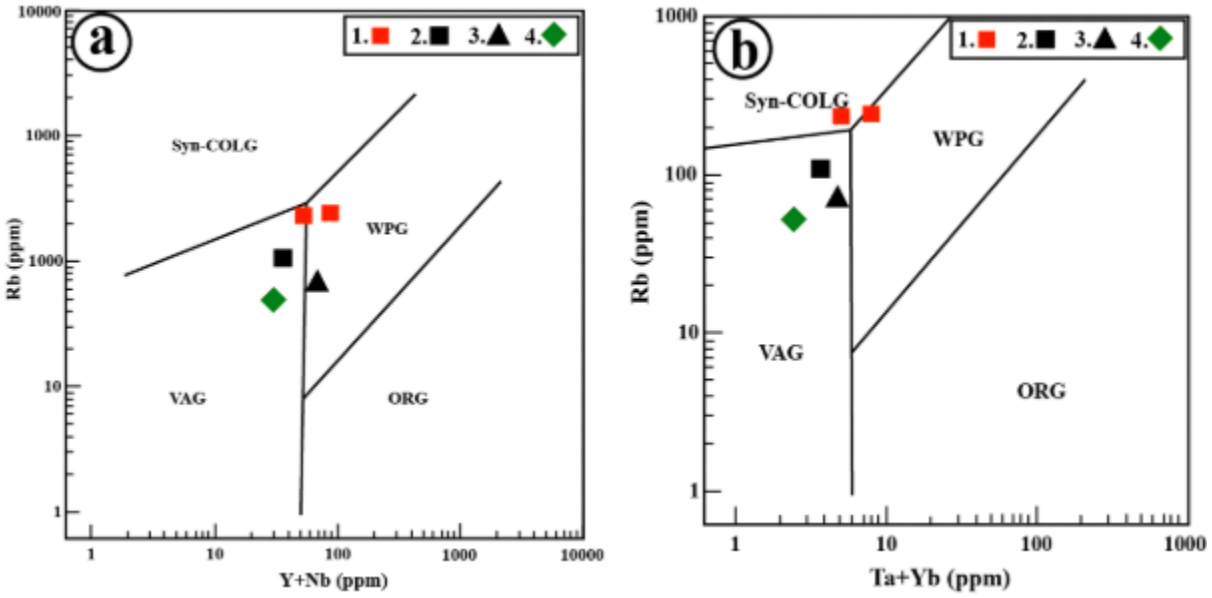


Figure 10

Tectonic discrimination diagrams of [46] for the Makassa rock. **a.** Rb versus (Y+Nb); **b.**Rb versus (Ta+Yb). **1.**amphibole-biotite granite; **2.** Biotite granite; **3.** Gneiss; **4.** Amphibolite.